ChemPubSoc Europe

DOI: 10.1002/cssc.201403364

CHEMSUSCHEM Communications

Carbon-Supported Base Metal Nanoparticles: Cellulose at Work

Jacco Hoekstra,[a] Marjan Versluijs-Helder,[b] Edward J. Vlietstra,[a] John W. Geus,[a] and Leonardus W. Jenneskens*[a]

Pyrolysis of base metal salt loaded microcrystalline cellulose spheres gives a facile access to carbon-supported base metal nanoparticles, which have been characterized with temperature-dependent XRD, SEM, TEM, ICP-MS and elemental analysis. The role of cellulose is multifaceted: 1) it facilitates a homogeneous impregnation of the aqueous base metal salt solutions, 2) it acts as an efficacious (carbonaceous) support material for the uniformly dispersed base metal salts, their oxides and the metal nanoparticles derived therefrom, and 3) it contributes as a reducing agent via carbothermal reduction for the conversion of the metal oxide nanoparticles into the metal nanoparticles. Finally, the base metal nanoparticles capable of forming metastable metal carbides catalytically convert the carbonaceous support into a mesoporous graphitic carbon material.

Metal nanoparticles (MNPs), which have a high surface-area-to-volume ratio, are widely studied owing to their (potential) catalytic, biomedical, optical, and electronic applications.[1] MNPs are commonly prepared by chemical reduction of metal salts. Because metal atoms at the surface of MNPs are mobile even at moderate temperatures,[2] contacts between the MNPs must be restricted in order to prevent sintering and maximize the accessible surface area. In heterogeneous catalysis MNPs are therefore supported on highly porous solid supports; for example, alumina, silica, or activated carbon (AC).[3] Usually, the metal salts are applied onto the support by impregnation or (deposition-)precipitation.[4] Subsequent reaction to supported MNPs involves drying, calcination, and hydrogen reduction.[5] Calcination, that is, treatment at elevated temperatures in air, is required to convert the dispersed MNP precursors to the metal oxides and to remove water from the loaded support. Hydrogen reduction of precious MNPs (e.g., platinum, palladium) already proceeds at RT and is not affected by water. AC is the support of choice for precious MNPs. It withstands highly alkaline and acidic liquids, while the precious metal can be easily recovered from the spent catalysts by combustion of the AC.[6]

With most base MNPs, AC cannot be employed. Calcination, which requires high temperatures with base metals, leads to oxidation of the AC and must be replaced by thermal treatment in an inert gas. Moreover, water may severely impede hydrogen reduction of the base metal oxides (e.g., copper, nickel, cobalt, iron).[7] With active hydrogenation catalysts such as nickel or cobalt,[8] hydrogen reduction leads to gasification of the AC as methane, which results in excessive sintering of the MNPs. In addition, the reduction is technically complicated due to the wide explosion limits of hydrogen.[9] Industrial utilization of AC supports has therefore remained limited to precious metals.

Here we report a facile procedure to obtain highly dispersed carbon-supported base MNPs in which the use of hydrogen gas as a reducing agent is avoided. We start with the impregnation of microcrystalline cellulose spheres (MCCs, particle size 100–200 μm)[10] with 2 M aqueous solutions of nitrate salts of copper, nickel, cobalt, or iron. The hydrophilic and porous character of the MCCs (cf. their application in the controlled release of drugs)[11] ensures facile impregnation. After filtration and drying the color throughout the volume of the spheres was identical to that of the impregnated salts, indicating a uniform distribution of the metal salts (Supporting Information, Figure S1). Realizing that during cellulose pyrolysis a reducing environment is created,[12] the loaded MCC spheres were pyrolyzed under a stagnant N_2 atmosphere at $T = 500\,^{\circ}C$, 600 °C, 700 °C, or 800 °C for 3 h in a tube furnace reactor (TFR; see Experimental Section).

After pyrolysis, black-colored bodies were obtained in all cases (Supporting Information, Figure S1) that retained their spherical shape and were uniform in size [ca. 70 μm as determined by scanning electron microscopy (SEM); Supporting Information, Figure S2 (left)]. The MNPs formed were imaged by using SEM-BSE [Figure S2 (right)]; high metal loadings were achieved (ICP–MS; Supporting Information, Table S1). The bodies initially loaded with a nickel, cobalt, or iron salt revealed ferromagnetic properties after pyrolysis at $T \geq 500\,^{\circ}C$ (see Supporting Information, Figure S3 and Table S1).

To monitor structural changes of the support and the supported metal cations during pyrolysis, temperature-dependent X-ray diffraction (TD-XRD; He 20 L h^{-1}, T = (RT–820 °C), 5 °C min^{-1}) was performed. To prevent contamination of the XRD reaction chamber with (volatile) tarry MCC decomposition

[a] Dr. J. Hoekstra, E. J. Vlietstra, Prof. Dr. J. W. Geus, Prof. Dr. L. W. Jenneskens
Organic Chemistry&Catalysis Debye Institute for Nanomaterials Science
Utrecht University
Universiteitsweg 99, 3584 CG Utrecht (The Netherlands)
Fax: (+31) 30-2523615
E-mail: l.w.jenneskens@uu.nl
Homepage: http://www.uu.nl/science/occ

[b] M. Versluijs-Helder
Inorganic Chemistry&Catalysis
Debye Institute for Nanomaterials Science
Utrecht University
Universiteitsweg 99, 3584 CG, Utrecht (The Netherlands)

Supporting Information for this article is available on the WWW under http://dx.doi.org/10.1002/cssc.201403364.

products, the samples were pretreated at $T=500\,^{\circ}C$ for 3 h (TFR, stagnant N_2(g), rate $5\,^{\circ}C\cdot min^{-1}$). After cooling to RT and exposure to ambient atmosphere TD-XRD was measured.

TD-XRD revealed that during pretreatment ($T=500\,^{\circ}C$) the copper cations are reduced to *fcc* copper NPs, which partly re-oxidize to Cu_2O upon exposure to ambient conditions (Figure 1 A, $T=25\,^{\circ}C$). At $T=388\,^{\circ}C$ the Cu_2O is again reduced to *fcc* copper (Figure 1 A). Intriguingly, the copper NP size (ca. 10 nm; Supporting Information, Figure S4 A), as calculated from the X-ray line broadening using the Scherrer equation (Supporting Information, Eq. S1), did not change over the whole temperature range. Note that reduction of copper catalysts in technical reactors is complicated due to the elevated heat of reaction. Hence, combining the endothermic decomposition of cellulose[13] with the exothermic reduction of the copper species[14] is highly attractive.

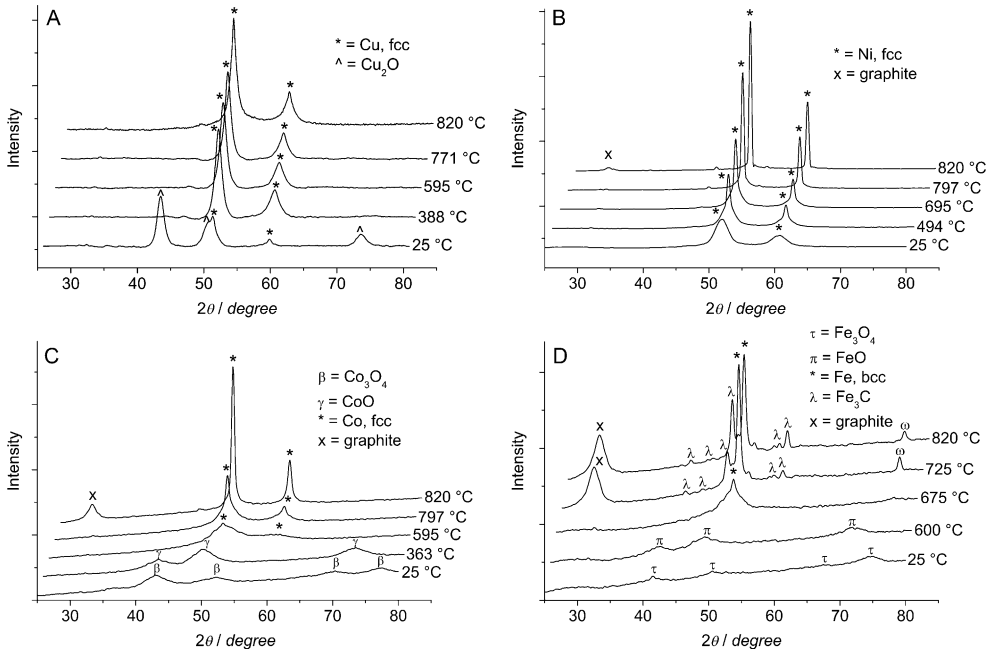

Figure 1. TD-XRD patterns of loaded MCC beads after pretreatment at $T=500\,^{\circ}C$. A) Copper, B) nickel, C) cobalt, and D) iron.

TD-XRD of the nickel-loaded beads after the thermal pretreatment ($T=500\,^{\circ}C$) showed full conversion of the nickel salt to *fcc* nickel NPs of ca. 8 nm (Figure 1 B, $T=25\,^{\circ}C$ and Figure S4 B). Surprisingly, no pyrophoricity was observed during exposure to ambient atmosphere. This suggests that the nickel NPs are protected from oxidation. Between $T=450$–$600\,^{\circ}C$ the nickel NP size increased up to ca. 45 nm followed by another increase up to ca. 65 nm above $T=700\,^{\circ}C$ (Figure S4 B). Concurrently, at $T=820\,^{\circ}C$ a new, albeit weak, diffraction maximum assigned to graphite (d_{002}) became discernible (Figure 1 B).

In contrast to the nickel-loaded beads, the cobalt-loaded beads were strongly pyrophoric after pretreatment ($T=500\,^{\circ}C$) upon exposure to ambient atmosphere, indicative of the presence of highly reactive cobalt NPs. TD-XRD (Figure 1 C, $T=25\,^{\circ}C$) revealed the presence of Co_3O_4 NPs (size ca. 7 nm, Figure S4 C), which at increasing temperature gave CoO NPs ($T=260$–$300\,^{\circ}C$, size ca. 6 nm) and finally *fcc* cobalt NPs ($T=475$–$570\,^{\circ}C$, size ca. 5 nm). At $T=820\,^{\circ}C$ a (d_{002}) graphite reflection appeared with higher intensity than observed for the carbon support in contact with nickel NPs. Concomitantly, the size of the cobalt NPs increased up to ca. 30 nm (Figure S4 C).

After pretreatment ($T=500\,^{\circ}C$) of the iron-loaded beads, magnetite (Fe_3O_4) NPs were identified [TD-XRD, Figure 1 D, $T=25\,^{\circ}C$, size ca. 6 nm (Figure S4 D)]. Raising the temperature induced a stepwise reduction to FeO NPs ($T=540$–$570\,^{\circ}C$, size ca. 5 nm) and finally to *bcc* iron NPs ($T=620$–$700\,^{\circ}C$; size ca. 10 nm). In addition, above $T=700\,^{\circ}C$ cementite (Fe_3C) reflections were discernible, indicative of carbon uptake by the iron NPs. Concurrently, an intense graphite reflection (d_{002}) and a further increase in iron NP size up to ca. 50 nm were observed.

Clearly, reduction of the metal oxide NPs into reduced NPs does not require an external reductant, viz. hydrogen. Elemental analysis of pristine MCC spheres after pyrolysis at $T=500$–$800\,^{\circ}C$ revealed the formation of a highly carbonaceous support (Supporting Information, Table S2), pointing to a carbothermal reduction process.[15] Presumably the intimate contact between the metal oxide NPs and the carbon support ensures a smooth reduction.

TEM images showed that the copper NPs are uniformly distributed throughout the spheres after pyrolysis at either $T=500\,^{\circ}C$ or $T=800\,^{\circ}C$ (Figure 2 A–B), which is in line with a uniform distribution of the copper salt throughout the MCC spheres upon impregnation. The copper NP size is independent of the pyrolysis temperature, which is consistent with the XRD results. The cellulose has been converted to an amorphous carbon [HR-TEM; wavy pattern (Figure 2 C and Supporting Information, Figure S5)]. The image shows some copper NPs present within the amorphous carbon after pyrolysis at $T=800\,^{\circ}C$. This is consistent with the conversion of crystalline cellulose into an amorphous carbon upon pyrolysis at this temperature.[16] We attribute the thermostability of the copper NPs to a restricted mobility over the atomically rough surface of the amorphous carbon support hampering sintering.

Reduced nickel NPs were observed by STEM-HAADF (the bright spots indicating species of a heavier element viz. nickel) after treatment at $T=500\,^{\circ}C$ according to EDX elemental analysis (Figure 3 A). The nickel NPs are encapsulated in thin graphitic shells (HR-TEM, Figure 3 B), which explains the absence of pyrophoric behavior and, so, the absence of nickel oxide.

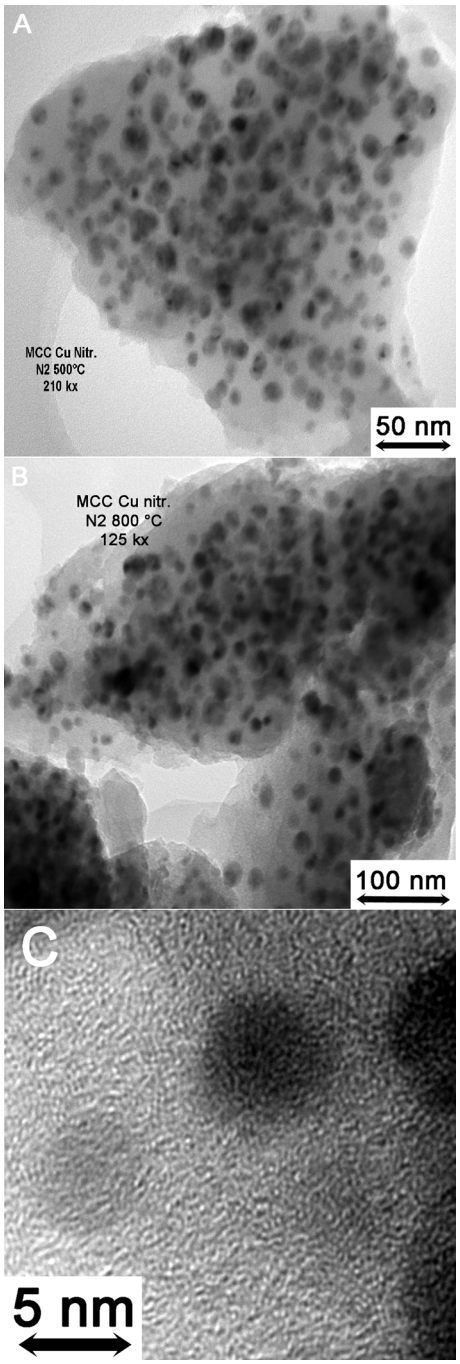

Figure 2. TEM images of carbon-supported copper NPs after pyrolysis at A) $T=500\,^{\circ}C$, and B) $T=800\,^{\circ}C$. C) HR-TEM image of copper NPs embedded in amorphous carbon ($T=800\,^{\circ}C$).

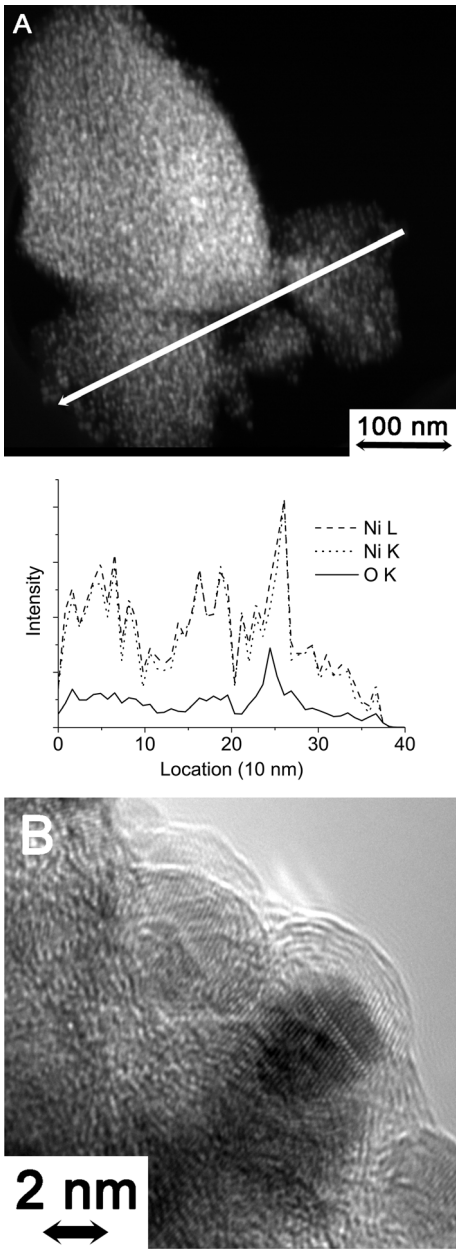

Figure 3. A) STEM-HAADF image with EDX elemental analysis along the arrow of carbon-supported nickel NPs after pyrolysis at $T=500\,^{\circ}C$, and B) HR-TEM image of a thin graphitic shell surrounding a nickel NP. The lattice fringes of nickel are also visible.

The obtained cobalt NPs were pyrophoric after treatment at $T=500\,^{\circ}C$ and $T=600\,^{\circ}C$, which indicates that a reaction to very small and, hence, highly reactive cobalt NPs must have proceeded. Provided the pyrolysis temperature is sufficiently high ($T>600\,^{\circ}C$), the cobalt NPs (TEM, Figure 4A) become encapsulated in a thin graphitic shell (HR-TEM, Figure 4B), similar to nickel (Figure 3B), the difference being that the shells in the case of cobalt NPs are formed at a higher temperature.

Figure 5 shows STEM-HAADF images of the iron-loaded spheres after pyrolysis at $T=500\,^{\circ}C$ and $T=800\,^{\circ}C$. A uniform distribution of iron oxide NPs [according to energy dispersive X-ray (EDX) analysis] throughout the spheres was obtained after treatment at $T=500\,^{\circ}C$ (Figure 5A). Larger NPs are observed after treatment at $T=800\,^{\circ}C$ (Figure 5B, size ca. 20–70 nm), which agrees satisfactorily with the NP size calculated from the X-ray line broadening (Figure S4D). The reduction to metallic iron is evident; a much lower oxygen emission intensity is found (EDX). The recrystallization of the initial amorphous carbon to graphitic carbon is apparent from the curved graphitic layers in Figure 5C (TEM) and D (HR-TEM). The difference with the amorphous carbon resulting from the pyrolysis of copper-loaded MCC beads (Figure 2C) is striking.

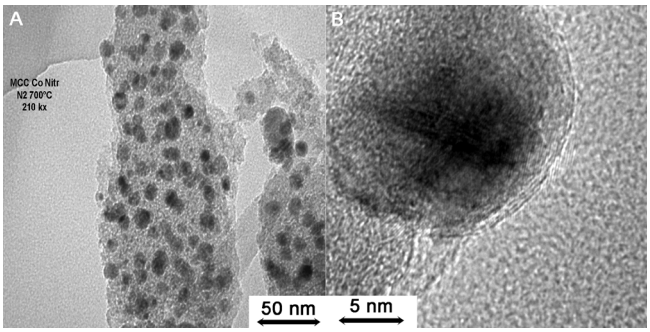

Figure 4. A) TEM image of carbon-supported cobalt NPs after pyrolysis at $T = 700\,^{\circ}C$, and B) HR-TEM image of a graphitic shell surrounding a cobalt NP.

Nickel, cobalt, and iron, capable of forming metastable metal carbides,[17] are known graphitization catalysts.[18] The amorphous carbon can diffuse into the metal, yielding metal carbides, which subsequently decompose into graphitic carbon and the metal.[19] Because graphite has a smooth surface in contrast to amorphous carbon, the reaction to graphitic carbon leads to metallic NPs with a high surface mobility and, consequently, to a rapid sintering of the MNPs. The copper NPs, unable to form carbides[17] therefore do not sinter. This is substantiated by histograms of the particle size distributions of the copper- and iron-loaded spheres after pyrolysis at $T = 800\,^{\circ}C$, derived from STEM-HAADF images (Supporting Information, Figure S6).

A variety of applications for the (graphitic) carbon-supported base MNPs are foreseen, such as in catalysis, (e.g., cobalt and iron in Fischer–Tropsch),[20] as active adsorbents in remediation (zero-valent iron),[21] and as biocides [copper(oxide)].[22] Clearly, a prerequisite for these applications is the accessibility of the NP surface for either gaseous and/or liquid reactants, which is governed by the textural properties (surface area, porosity) of the metal–carbon composites. Therefore, the textural properties of the samples obtained after pyrolysis were measured with nitrogen physisorption (Supporting Information, Table S3). Pyrolysis of pristine MCC in the absence of a metal salt led to a non-porous carbon material. In the presence of metal salts, however, microporous carbon supports were obtained with a surface area up to $500\,m^2\,g^{-1}$. Remarkably, upon reduction of the metals capable of forming metastable metal carbides (nickel, cobalt, iron) and subsequent graphitization, the surface area is lowered. During transformation of the amorphous carbon to graphitic carbon, mesopores are formed at the expense of micropores, which is most pronounced in the case of cobalt and iron. The wider mesopores improve diffusion within the graphitic carbon body.[23] The facile formation of Cu_2O (Figure 1 a), Co_3O_4 (Figure 1 c), and Fe_3O_4 (Figure S6), respectively, upon exposure to ambient at-

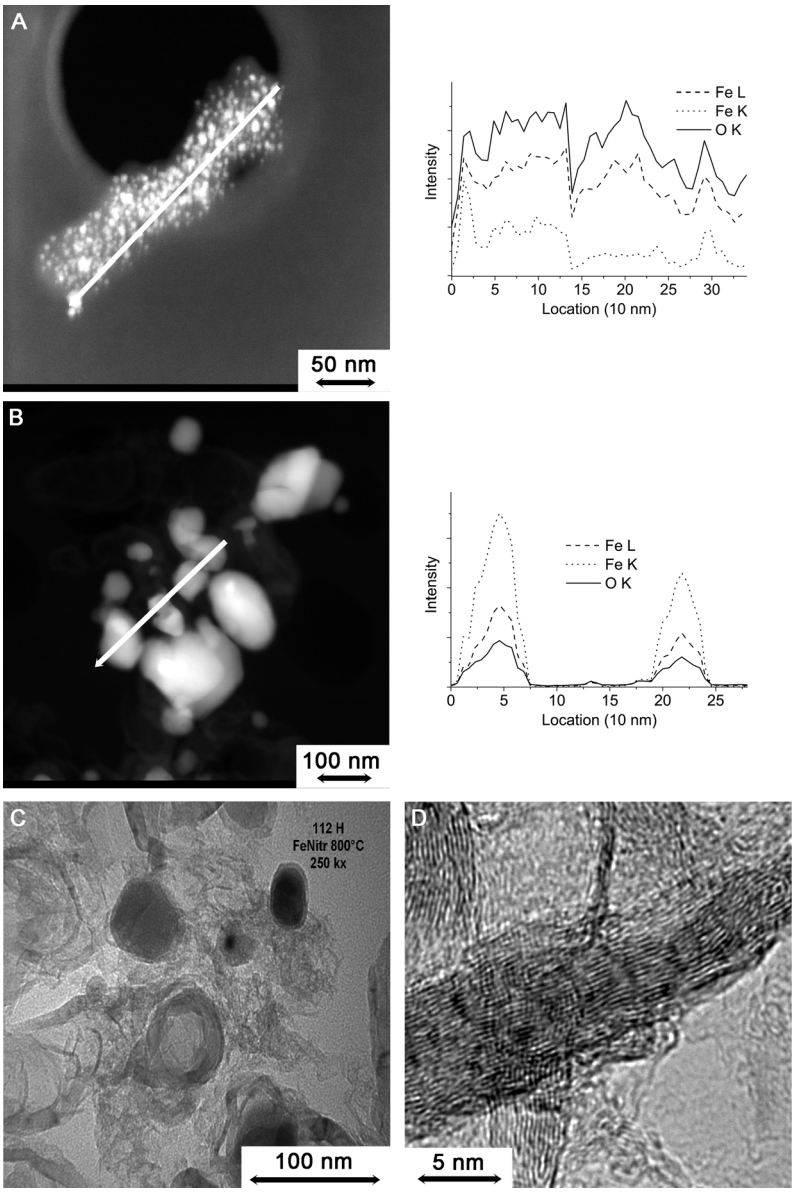

Figure 5. A) STEM-HAADF image with EDX elemental analysis of supported iron oxide NPs after pyrolysis at $T = 500\,^{\circ}C$, B) STEM-HAADF image with EDX elemental analysis of supported iron NPs after pyrolysis at $T = 800\,^{\circ}C$, C) TEM image, and D) HR-TEM image of graphitic carbon.

mosphere testifies to the accessibility and reactivity of the obtained copper, cobalt, and iron NPs with gaseous reactants. The rapid characteristic color change of a 4 M aqueous HCl solution in the presence of the carbon-supported base MNPs (copper→green, nickel→light green, cobalt→light pink, iron→yellow; Supporting Information, Figure S7) shows the accessibility of the MNPs for liquid reactants.

In summary, base metal nanoparticles (MNPs) uniformly dispersed throughout carbonaceous supports are readily accessible by pyrolysis of base-metal-salt-loaded microcrystalline cellulose (MCC) spheres. This method provides a number of benefits, both from a preparative as well as from an application perspective: 1) the cellulose acts as a carbothermal reductant, avoiding the use of hydrogen gas; 2) a supreme MNP dispersion is achieved; 3) the extensive heat of reduction of copper catalysts is dissipated by the endothermic decomposition of the cellulose; 4) catalytic graphitization (nickel, cobalt, iron) leads to an enhanced porosity as well as 5) an improved stability against oxidation of the support; and 6) in view of the industrially relevant Fischer–Tropsch reaction (iron and cobalt), the large amounts of water produced will be easily released from the graphitized hydrophobic carbon (cf. also Supporting Information, Table S4).

Experimental Section

MCC spheres (50 g) were immersed for 24 h in 2 M aqueous solutions (100 mL) of the metal salts employed (nitrate salts of copper, nickel, cobalt or iron) under occasional stirring. After filtration (Büchner funnel with glass filter) and drying in vacuo ($p = 10^{-2}$ mbar) the dried (loaded) spheres (5 g) were pyrolyzed in a stagnant inert N_2 (g) atmosphere in a tube furnace reactor (TFR). Prior to pyrolysis the TFR was evacuated and refilled with N_2 (g) thrice. Next, the TFR was heated (rate 5 °C·min^{-1}) to the desired temperature (T 500 °C, 600 °C, 700 °C or 800 °C), followed by isothermal pyrolysis for 3 h. After cooling to RT the product was exposed to ambient atmosphere. For more details and characterization procedures see Supporting Information.

Acknowledgements

*We thank AgentschapNL for financial support (*in situ *H_2O_2, project IS 043063). We further acknowledge Dr. P.H. Berben and Dr. D. van de Kleut from BASF Nederland B.V. for access to experimental facilities and valuable discussions.*

Keywords: carbon · cellulose · graphite · nanoparticles · reduction

[1] a) A.-H. Lu, E. L. Salabas, F. Schüth, *Angew. Chem. Int. Ed.* **2007**, *46*, 1222 – 1244; *Angew. Chem.* **2007**, *119*, 1242 – 1266; b) P. K. Jain, X. Huang, I. H. El-Sayed, M. A. El-Sayed, *Acc. Chem. Res.* **2008**, *41*, 1578 – 1586; c) S. K. Ghosh, T. Pal, *Chem. Rev.* **2007**, *107*, 4797 – 4862; d) D. Astruc, F. Lu, J. R. Aranzaes, *Angew. Chem. Int. Ed.* **2005**, *44*, 7852 – 7872; *Angew. Chem.* **2005**, *117*, 8062 – 8083.
[2] J. A. Moulijn, A. E. van Diepen, F. Kapteijn, *Appl. Catal. A* **2001**, *212*, 3 – 16.
[3] Z. Ma, F. Zaera, *Heterogeneous Catalysis by Metals, Encyclopedia of Inorganic Chemistry*, Wiley-VCH, Weinheim, **2006**.
[4] R. J. White, R. Luque, V. L. Budarin, J. H. Clark, D. J. Macquarrie, *Chem. Soc. Rev.* **2009**, *38*, 481 – 494.
[5] G. Ertl, *Preparation of Solid Catalysts*, Wiley-VCH, Weinheim, **1999**.
[6] F. Rodríguez-Reinoso, *Carbon* **1998**, *36*, 159 – 175.
[7] J. Zielinski, I. Zglinicka, L. Znak, Z. Kaszkur, *Appl. Catal. A* **2010**, *381*, 191 – 196.
[8] C. I. Meyer, S. A. Regenhardt, A. J. Marchi, T. F. Garetto, *Appl. Catal. A* **2012**, *417 – 418*, 59 – 65.
[9] V. Schröder, B. Emonts, H. Janßen, H.-P. Schulze, *Chem. Eng. Technol.* **2004**, *27*, 847 – 851.
[10] Cellets 100, Syntapharm GmBh, Mülheim an der Ruhr, Germany.
[11] G. Majid Khan, J.-B. Zhu, *J. Controlled Release* **1999**, *57*, 197 – 203.
[12] V. Mamleev, S. Bourbigot, J. Yvon, *J. Anal. Appl. Pyrolysis* **2007**, *80*, 141 – 150.
[13] U.-J. Kim, S. H. Eom, M. Wada, *Polym. Degrad. Stab.* **2010**, *95*, 778 – 781.
[14] M. H. Yamukyan, K. V. Manukyan, S. L. Kharatyan, *J. Alloys Compd.* **2009**, *473*, 546 – 549.
[15] G. Chieffi, C. Giordano, M. Antonietti, D. Esposito, *J. Mater. Chem. A* **2014**, *2*, 11591 – 11596.
[16] D.-Y. Kim, Y. Nishiyama, M. Wada, S. Kuga, *Carbon* **2001**, *39*, 1051 – 1056.
[17] C. P. Deck, K. Vecchio, *Carbon* **2006**, *44*, 267 – 275.
[18] J. Jiao, S. Seraphin, X. K. Wang, J. C. Withers, *J. Appl. Phys.* **1996**, *80*, 103 – 108.
[19] a) W. Lu, W. C. Mitchell, G. R. Landis, T. R. Crenshaw, W. Eugene Collins, *Solid State Electron.* **2003**, *47*, 2001 – 2010; b) S. Glatzel, Z. Schnepp, C. Giordano, *Angew. Chem. Int. Ed.* **2013**, *52*, 2355 – 2358; *Angew. Chem.* **2013**, *125*, 2411 – 2414.
[20] H. M. Torres Galvis, J. H. Bitter, C. B. Khare, M. Ruitenbeek, A. I. Dugulan, K. P. de Jong, *Science* **2012**, *335*, 835 – 838.
[21] a) K. Mackenzie, S. Bleyl, A. Georgi, F.-D. Kopinke, *Water Res.* **2012**, *46*, 3817 – 3826; b) L. B. Hoch, E. J. Mack, B. H. Hydutsky, J. M. Hershman, J. M. Skluzacek, T. E. Mallouk, *Environ. Sci. Technol.* **2008**, *42*, 2600 – 2605.
[22] J. P. Ruparelia, A. K. Chatterjee, S. P. Duttagupta, *Acta Biomater.* **2008**, *4*, 707 – 716.
[23] T. J. Bandosz, *Activated Carbon Surfaces in Environmental Remediation*, Elsevier, Amsterdam, **2006**.

Received: December 4, 2014
Published online on February 20, 2015